BIOCHEMISTRY
including biophysical chemistry & molecular biology

Article

pubs.acs.org/biochemistry

Characterization of Binding Mode of Action of a Blocking Anti-Platelet-Derived Growth Factor (PDGF)-B Monoclonal Antibody, MOR8457, Reveals Conformational Flexibility and Avidity Needed for PDGF-BB To Bind PDGF Receptor-β

Jun Kuai,[#,†] Lidia Mosyak,[#,†] Jon Brooks,[†] Michael Cain,[†] Gregory J. Carven,[‡] Shinji Ogawa,[§] Tetsuya Ishino,[†] May Tam,[†] Edward R. Lavallie,[†] Zhiyong Yang,[†] Dirk Ponsel,[∥] Robert Rauchenberger,[⊥] Robert Arch,[¶] and Nick Pullen*[,†]

[†]Pfizer Global Research & Development, 610 Main Street, Cambridge, Massachusetts 02139, United States

[‡]Scholar Rock LLC, 300 Technology Square, Cambridge, Massachusetts 02142, United States

[§]Pfizer Japan Inc., 3-22-7 Yoyogi, Shibuya, Tokyo 151-8589, Japan

[∥]Roche Diagnostics GmbH, Nonnenwald 2, 82377 Penzberg, Germany

[⊥]MorphoSys AG, Lena-Christ Strasse 48, 82152 Martinsried, Germany

[¶]Takeda Pharmaceuticals International Inc., One Takeda Parkway, Deerfield, Illinois 60015, United States

Supporting Information

ABSTRACT: Platelet derived growth factor-BB (PDGF-BB) is an important mitogen and cell survival factor during development. PDGF-BB binds PDGF receptor-β (PDGFRβ) to trigger receptor dimerization and tyrosine kinase activation. We present the pharmacological and biophysical characterization of a blocking PDGF-BB monoclonal antibody, MOR8457, and contrast this to PDGFRβ. MOR8457 binds to PDGF-BB with high affinity and selectivity, and prevents PDGF-BB induced cell proliferation competitively and with high potency. The structural characterization of the MOR8457-PDGF-BB complex indicates that MOR8457 binds with a 2:1 stoichiometry, but that binding of a single MOR8457 moiety is sufficient to prevent binding to PDGFRβ. Comparison of the MOR8457-PDGF-BB structure with that of the PDGFRβ-PDGF-BB complex suggested the potential reason for this was a substantial bending and twisting of PDGF-BB in the MOR8457 structure, relative to the structures of PDGF-BB alone, bound to a PDGF-BB aptamer or PDGFRβ, which makes it nonpermissive for PDGFRβ binding. These biochemical and structural data offer insights into the permissive structure of PDGF-BB needed for agonism as well as strategies for developing specific PDGF ligand antagonists.

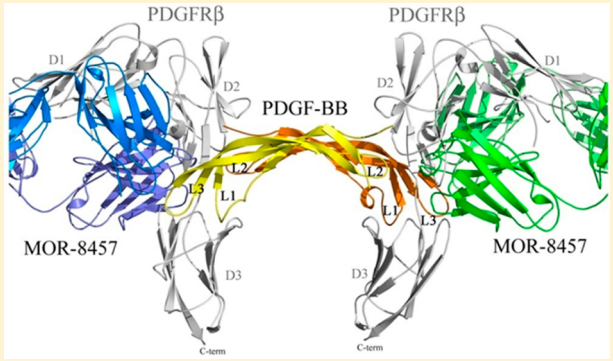

PDGFs are the primary mitogens for the cells of the mesenchymal and neuroectodermal origin. The PDGF family is composed of four different polypeptide chains, PDGF-A, -B, -C, and -D, which have been shown to form five distinct proteins by homo- and heterodimerization, PDGF-AA, -AB, -BB, -CC, and -DD. PDGFs exert their biological effect by activating two structurally related tyrosine kinase receptors, PDGFRα and β, which form homo- and heterodimers (e.g., PDGFR$\alpha\alpha$, PDGFR$\alpha\beta$, PDGFR$\beta\beta$). PDGF-AA activates PDGFR$\alpha\alpha$, while PDGF-BB can activate all three receptor dimers, i.e., PDGFR$\alpha\alpha$, PDGFR$\alpha\beta$, and PDGFR$\beta\beta$. PDGF-AB and PDGF-CC activate PDGFR$\alpha\alpha$ and PDGFR$\alpha\beta$, whereas PDGF-DD preferentially activates PDGFR$\beta\beta$.[1−3]

PDGFs have been implicated in a wide variety of human diseases, including atherosclerosis, pulmonary hypertension, retinal vascular disease, organ fibrosis (e.g., cardiac, lung and kidney), tumorigenesis, and systemic sclerosis.[1,3] All four PDGF isoforms, as well as both receptor chains, are expressed in the kidney, and increased expression in glomerular and/or interstitial locations has been documented in a large variety of human renal diseases and experimentally.[2,4−9] Both PDGF-B and PDGF-D appear to be especially important in human renal diseases.[4,10−16] Mesangial cells produce PDGF-B in vitro, and various growth factors induce mesangial proliferation via induction of autocrine or paracrine PDGF-B-chain excretion.[17−21] Overexpression of PDGF-B-chain induces mesangial proliferation and matrix expansion.[17,22,23] In contrast, disruption of the PDGF-B or PDGFRβ genes in mice leads to the

Received: December 19, 2014
Revised: February 20, 2015
Published: February 24, 2015

DOI: 10.1021/bi5015425
Biochemistry 2015, 54, 1918−1929

development of lethal hemorrhage and edema in late embryogenesis and absence of kidney glomerular mesangial cells.[24−26] Specific inhibition of PDGF-B using antibodies, aptamers, soluble PDGF receptors, or PDGFRβ tyrosine kinase blockers reduces mesangioproliferative changes, prevents long-term renal scarring, and improves renal function in a number of different preclinical models.[27−32] Similar observations of PDGF-B upregulation and involvement have been inferred from expression studies and experimental studies of liver as well as cardiac fibrotic conditions,[3,33−37] which when taken together underscores the importance of targeting PDGF-B to limit undesirable extracellular matrix deposition and to retain organ function.

This study was undertaken to understand the structure−function properties of a newly identified blocking PDGF-B monoclonal antibody, MOR8457. Our biophysical characterization as well as the structural determination of the complex offers unique insights to the specificity of the PDGFRβ-PDGF-BB interaction and the role of the conformation of the L1 and L3 loops in mediating permissive contacts with PDGFRβ needed for receptor agonism.

EXPERIMENTAL PROCEDURES

Identification of MOR8457. The anti-PDGF mAb MOR8457 was identified using solution phase panning of the MorphoSys HuCAL GOLD phagemid library.[38] Fabs were screened for selectivity to human PDGF-BB, crossreactivity to mouse PDGF-BB and blockade of binding to PDGFRβ in biochemical based binding assays. Fab hits were selected based on the ability to neutralize receptor phosphorylation by PDGF-BB using PDGFRβ stably transfected PAE cells. MOR8457 Fab was selected as a potent inhibitor of PDGFRβ signaling.

Selection of MOR8457. Four rounds of RapMAT solution panning[39] were performed using biotinylated, recombinant human PDGF-BB (Biosource Int. Inc.). To increase the affinity of specific clones, the output from the second round of panning was subjected to CDR-H2 diversification. For this, the respective CDR-H2 insert was released via restriction digest from the Fab-encoding plasmid DNA. The vector backbones were ligated with HuCAL CDR-H2 cassettes and transformed into *Escherichia coli* Top10F cells. Phages of the generated libraries were subjected to two additional rounds of solution pannings under very stringent conditions to select for high affinity.[40]

To facilitate rapid expression of soluble Fab, the Fab encoding inserts of the selected phages were subcloned into the pMORPHx9_MH expression vector.[41] After transformation of *E. coli* TG1 F- single clone expression and generation of *E. coli* crude bacterial extracts containing HuCAL GOLD Fab fragments were performed as described previously.[42]

Screening of MOR8457. PDGF-BB positive clones were identified by screening clones for antigen binding using ELISA as well as functional PDGF-BB inhibitory activity using a receptor inhibition assay in parallel.

For ELISA, human PDGF-BB (5 μg/mL in PBS) was coated to 384-well microtiter plates at 4 °C. After overnight incubation, coated plates were washed with PBS-T (PBS/0.05% Tween20) and blocked with 5% MPBS-T (5% milk powder in PBS-T) for 1 h. After several washing steps primary antibodies in *E. coli* crude extracts were added and incubated for 1 h. After washing, the secondary antibody (goat antihuman $F(ab)_2$ - fragment specific - AP labeled, Jackson) was added for 1 h. Subsequently plates were washed with TBS T, AttoPhos Substrate (Roche) was added, and fluorescence emission at 535 nm was recorded with excitation at 430 nm.

Inhibition of PDGFRβ binding was assessed on 384-well MSD plates coated with 2.5 μg/mL PDGFRβ-Fc fusion protein (R&D Systems) overnight at 4 °C. *E. coli* crude extract containing the Fab fragments was incubated with biotin-PDGF-BB (30 ng/mL) and transferred to the plates. After incubation for 1 h and washing with BV buffer (PBS/0.02% Tween 20/0.5% BSA) plates were incubated for 1 h with Streptavidin-BV. After washing with BV-buffer and addition of MSD read buffer detection was performed using a MSD MA6000 device.

Blockade of PDGFRβ receptor phosphorylation by PDGF-BB ligand was analyzed using PAE cells stably transfected with PDGFRβ. Cells were cultured in culture medium (F12 Nutrient Ham medium with L-glutamine supplemented with 10% FBS (PAN Biotech), 2 mM L-glutamine, and 500 μg/mL Geneticin (PAA). 5×10^5 cells/well were seeded into 96-well plates and incubated for 6 h. Culture medium was exchanged to starving medium (culture medium cont. 0.1% FBS) and incubated overnight. Different concentrations of antibodies (30 nm to 1.5 pM) were incubated with 0.4 nM PDGF-BB (final concentration) diluted in starving medium. Supernatant of cells was discarded, and antibody-PDGF-BB complexes were added to the cells. After exactly 10 min at 37 °C, cells were washed once with ice cold PBS followed by cell lysis using MSD cell lysis buffer. Phosphorylation of Tyr751 of PDGFRβ was quantified using MSD Multispot PDGFRβ whole cell lysis kit (Mesoscale Discovery) using the manufacturer's protocol.

Expression and Purification of MOR8457. DNA encoding the variable domain fragments of the heavy (VH) and light chains (VL) of MOR8457 was codon optimized for expression in mammalian cells and subcloned into expression vectors for transient expression. Depending on the application, the constant regions consisted of mouse IgG1, or human IgG1 containing mutations to abrogate binding to FcγR.[43] Human MOR8457-hIgG1 was stably expressed in Chinese hamster ovary (CHO) cells. CHO DUKX cells were stably transfected using separate expression plasmids for the heavy and light chains. Stable pools were selected with G418 and methotrexate for 2−3 weeks and scaled appropriately for expression. Antibody was purified using protein A chromatography followed by size exclusion to remove aggregates and formulated in PBS. Chimeric MOR8457-mIgG1 was produced via transient transfection using the HEK293 Freestyle system by Sino Biological (Beijing, China).

Expression and Purification of PDGFRβ-ECD-hIgG1. A synthetic DNA expression construct encoding an immunoglobulin Fc fusion protein consisting of the first three immunoglobulin-like extracellular domains (ECD) of PDGFRβ fused via linker to human IgG1 and termed PDGFRβ-ECD-hIgG1 was created via commercial gene synthesis. PDGFRβ-ECD-hIgG1 was stably expressed in CHO DUKX cells. CHO cells were transfected as above and stable clones were selected with methotrexate for 2−3 weeks. PDGFRβ-ECD-hIgG1 was purified using protein A chromatography followed by size exclusion. Purified Fc fusion protein was formulated in PBS. A monomeric variant of PDGFRβ-ECD-hIgG1, Fab-hIgG1-PDGFR(D1-D3), generated by fusing the first three immunoglobulin-like extracellular domains of PDGFRβ to an anti-VEGF Fab was constructed utilizing engineered N-glycosylation sites within the Fc region to prevent Fc homodimerization.[44] Monomeric variants were expressed and purified as above using protein A chromatography.

DOI: 10.1021/bi5015425
Biochemistry 2015, 54, 1918−1929

Expression and Purification of PDGF-BB. A cDNA sequence for mature human PDGF-B representing amino acids 82−190 of NP_002599.1, appended with a 5′ initiator methionine codon and a 3′ stop codon, was prepared by DNA synthesis and inserted into pET16b vector for expression in *E. coli*. For protein production, the hPDGF-B/pET16b expression vector was used to transform *E. coli* host strain BL21 (DE3) (Novagen) and grown at 37 °C 250 rpm in LB medium containing 100 μg/mL ampicillin. When the OD600 of the culture reached 0.5, protein expression was induced by the addition of IPTG (0.5 mM, 4 h). The cells were harvested by centrifugation (4000*g*, 15 min, 4 °C) and stored at −80 °C until needed. The yield of cell mass was approximately 2 g of cells (wet weight) per liter of culture medium.

A portion of the frozen cell pellet (5 g) was resuspended in 200 mL of lysis buffer (20 mM Tris pH 8.0, 100 mM NaCl, 3 U/mL RNase, 40 U/mL DNase, three tablets protease inhibitor cocktail (Roche) and passed three times through a microfluidizer at 1000 bar. The cell lysate was centrifuged at 4 °C (9700*g*, 20 min), and the resulting pellet was resuspended in 250 mL of W1 buffer (20 mM Tris pH 8.0, 100 mM NaCl). The W1 suspension was centrifuged at 4 °C (9700*g* for 20 min), and the resulting pellet was resuspended in W1 buffer with 0.1% Triton X-100 (250 mL). The suspension was stirred at room temperature for 30 min, centrifuged at 4 °C (9700*g*, 20 min), and the process twice repeated. The resulting pellet was resuspended with 20 mM Tris pH 8.0, 1 M NaCl (250 mL), and the final IB pellet was collected by centrifugation at 4 °C (9700*g* for 20 min), and resuspended with W1 buffer (5 mL). A 2 mL portion of the purified inclusion bodies was solubilized with 20 mM Tris pH 8.0, 10 mM EDTA, 6 M guanidine HCl, 10 mM DTT and stirred at 4 °C for 4 h followed by centrifugation (15000*g*, 30 min). The clarified supernatant was loaded onto a 2 mL Source 30 RPC column (GE Healthcare) equilibrated with 0.1% TFA/H_20. PDGF was eluted by a gradient 0.1% TFA/H_20/AcCN to 60% (1 mL/min) over 20 column volumes. Fractions containing PDGF were pooled and diluted to 0.1 mg/mL with 20 mM Tris pH 8.0, 5 mM EDTA buffer. The protein was supplemented with 5 mM/0.5 mM reduced/oxidized glutathione, stirred for 1 h at RT, and then dialyzed against 20 mM Tris pH 8.0/5 mM EDTA buffer overnight at RT to promote dimerization. The PDGF was then concentrated to ∼0.5 mg/mL using a 10 K molecular weight cutoff concentrator (Millipore).

Generation of MOR8457 Fab. MOR8457 was concentrated to 2 mg/mL and dialyzed against 20 mM Tris pH 8.0, 10 mM EDTA overnight at 4 °C. The antibody solution was supplemented with cysteine-HCl to a final concentration of 20 mM and incubated with immobilized papain resin for 3 h at 37 °C. The digest was removed from the resin and dialyzed overnight against 5 mM sodium phosphate pH 7.0. A 2 mL CHT column (BioRad) was equilibrated with 5 column volumes of 250 mM sodium phosphate (pH 7.0), followed with 5 column volumes 5 mM sodium phosphate (pH 7.0), and the dialyzed material was loaded onto the column. A gradient elution was performed at 1 mL/min to 100% 250 mM sodium phosphate (pH 7.0) over 40 column volumes. Fractions containing Fab were pooled.

Crystallization, Data Collection, and Structure Determination. A molar ratio of 3:1 (PDGF/Fab) was used for generating the complex. A higher molar ratio was required due to the heterogeneous mixture of monomer and dimer PDGF-BB. Final purification of the complex was performed using a HiLoad Superdex 200 16/60 column (GE Healthcare) equilibrated with TBS. Fractions containing the complex were pooled and concentrated to >7 mg/mL for crystallographic studies. PDGF-BB in complex with MOR8457-Fab was crystallized at 18 °C from a solution containing 22% PEG 3350 and 0.1 M Tris, pH 7.0. The crystals had symmetry consistent with monoclinic space group $P2_1$ and contained one protein complex in the asymmetric unit cell. A data set to a 2.3 Å resolution was collected from a single frozen crystal at IMCA beamline 17-ID at the Argonne National Laboratory (APS). The data were processed and scaled using autoPROC[45] and SCALA.[46] The final data set was 99.7% complete with average redundancy of 3.4 and with R_{merge} of 4.4%. The structure is deposited in the RCSB Protein Data Bank (PDB ID 4QCI; RCSB ID RCSB085881).

The structure was solved by molecular replacement with PHASER[47] starting with the Fab fragment models prepared from the PDB entries: 2adg and 8fab, and with the PDGF-BB model prepared from entry: 3mjg. The initial solution was obtained by searching for each of the four domains of the Fab molecule separately. This partial solution was used to search for a second copy of the Fab fragment, followed by a final search for the PDGF-BB molecule. The final complete molecular replacement solution contained two Fab fragments bound to one PDGF-BB dimer. Several iterative rounds of model manual adjustment and model rebuilding using COOT followed by crystallographic refinement using autoBUSTER[48] yielded the final refined model of the complex with a crystallographic R_{work} of 21.1% and R_{free} of 24.8%. The final MOR8457-Fab+PDGF-BB model comprises two chains of the first Fab copy, H and L (residues 1H-133H, 142H- 191H, 200H-220H of heavy chain H and residues 3L-205L of light chain L), two chains of the second Fab copy, B and A (1B-134B, 141B-220B of heavy chain B and 2A-207A of light chain A) and two chains of PDGF-BB, C and D (10C-101C of chain C and 7D-102D of chain D). Missing amino acids in some regions were not modeled into the structure because of the lack of electron density, very likely due to disorder. Nonprotein atoms present in the model include 327 water molecules. Statistics for data collection and refinement are shown in Table 1, and the residue contacts described in Table 2. Statistics for data collection and refinement are shown in Table 1 and an example of the final electron density map is shown in Supplemental Figure 1, Supporting Information.

Structure Homology Modeling of PDGF-DD. An initial amino-acid sequence alignment between PDGF-B and the growth factor domain of PDGF-DD was produced with ClustalW resulting in ∼25% sequence identity.[49] This alignment was manually adjusted to match up the secondary structure of the proteins and to satisfy cysteine-pairs that form disulfide bridges in PDGF-BB. In the resulting alignment, four cysteine pairs were aligned with the corresponding conserved disulfide pattern of PDGF-BB, and one extra cysteine pair remained unmatched. This alignment together with the structure of PDGF-BB as a homologous template was then used to calculate 50 structural models of the PDGF-DD with Modeler.[50] Each model represented the PDGF-DD dimer structure containing the eight conserved and two new disulfides. The best model was selected on the basis of the lowest value of the Modeler objective function.

Binding Kinetics and Stoichiometry of MOR8457 and PDGFRβ-ECD-hIgG1 by BIAcore. All binding kinetic studies were performed at 25 °C using a BIAcore 2000 instrument (GE

DOI: 10.1021/bi5015425
Biochemistry 2015, 54, 1918−1929

Table 1. Data Collection and Refinement Statistics[a]

Data collection	
space group	$P2_1$
unit cell (a, b, c, α, β, γ) (Å, °)	90.15, 68.47, 95.25, 90, 97.56, 90
wavelength (Å)	1.000
resolution range (Å)	69.6−2.3 (2.42−2.3)
total reflections	172282 (25, 707)
unique reflections	51,241 (7,417)
completeness (%)	99.7 (99.9)
redundancy	3.4 (3.5)
$I/\sigma(I)$[b]	12.7 (1.1)
R_{merge}[c] (%)	4.4 (73.6)
Refinement	
resolution range (Å)	69.6−2.3 (2.36−2.3)
R_{work}[d] (%)	21.1 (24.2)
R_{free}[e] (%)	24.75 (26.3)
rmsd bond length (Å)	0.009
rmsd bond angle (deg)	1.19
average B-values (Å^2)	65.2
protein atoms	7759
solvent atoms	327
Ramachandran plot (%)	
favored	96.19
allowed	2.81
outliers	1.0

[a]Values in parentheses represent the corresponding values for the highest resolution shells. [b]$I/\sigma(I)$ = average I/average $\sigma(I)$. [c]Multiplicity-weighted R_{merge} = $|I_h - \langle I_h \rangle|/I_h$, where $\langle I_h \rangle$ is the average intensity over symmetry equivalents. [d]$R_{work} = ||F_{obs}| - |F_{calc}||/|F_{obs}|$. [e]$R_{free}$ is equivalent to R_{work}, but calculated for a randomly chosen 5% of reflections omitted from the refinement process.

Table 2. Description of the MOR8457-PDGF-BB Residue Contacts

MOR-8457 paratope
Heavy chain: Trp 47, Tyr 50, Leu 57, Tyr 59, Tyr 60 and Asp 62 from CDR-H2; Trp 102, Tyr 103, Gly 104 and Gly 105 from CDR-H3
Light chain: Gly 28, Ser 29, Tyr 30 and Phe 31 from CDR-L1; Asp 49, Asp 50 and Asn 65 from CDR-L2; Phe 90, Thr 91, His 92, Asn 93 and Ser 94 from CDR-L3.
PDGF-B epitope
Chain C: Leu 38, Val, 39 and Trp 40 from loop 1; Glu 71, Arg 73, Ile 75, Ile 77, Arg 79, Lys 80, Lys 81, Pro 82, Ile 83, Phe 84, Lys 85 and Lys 86 from Loop 3
Chain D: Asn 54 and Arg 56 from loop 2.

Healthcare, Piscataway NJ). Anti-human or anti-mouse IgG (GE Healthcare) antibodies that were immobilized in adjacent flow cells of a CM5 sensor chip between 8000 and 10,000 resonance units (RU) using amine coupling as directed by the manufacturer. MOR8457-hIgG1, PDGFRβ-ECD-hIgG1 or MOR8457-mIgG1 was diluted into PBS-NET (10 mM phosphate pH 7.4, 287 mM NaCl, 2.7 mM KCl, 3.2 mM EDTA, 0.01% Tween 20) to 1 μg/mL and injected independently over the respective anti-human or anti-mouse surface for 10 s resulting in a stable anti-PDGF surface between 50 and 100RU. Different concentrations (1, 0.5, and 0.25 nM) of each PDGF isoform, including human PDGF-AA, -AB, -BB, -DD, as well as rat PDGF-BB (all obtained from R&D systems, Minneapolis, MN) and mouse PDGF-BB (Invitrogen, Carlsbad, CA) were injected over the antibody surface for 2 min at a flow rate of 100 μL/min. The complex was allowed to dissociate for 10 min. The surface was regenerated with a 30 s injection of 10 mM magnesium chloride leaving the surface ready for another round of anti-PDGF antibody capture and PDGF binding kinetics. Kinetic data were double referenced[51] using scrubber2 software (Bio-Logic Software) and then fit to a 1:1 binding model using BIAcore evaluation software version 4.1.

For determining the stoichiometry of MOR8457 binding, MOR8457-mIgG1 was captured by the anti-mouse IgG (GE Healthcare) immobilized onto a CM5 sensor chip using amine coupling resulting in a stable surface of 200-400RU. Human PDGF-BB (1 nM) was injected for 6 min until saturation and then followed by injection of MOR8457-hIgG1, PDGFRβ-ECD-hIgG1, or buffer. A monomeric variant of PDGFRβ-ECD-hIgG1 generated by fusing the first three immunoglobulin-like extracellular domains of PDGFRβ to an anti-VEGF Fab, termed Fab-hIgG1-PDGFR(D1-D3), was also injected to the surface of preassembled MOR8457-mIgG1/PDGF-BB complex as described above to test binding.

Mesangial Cell Proliferation Assays. Primary human mesangial cells (ScienCell Research, Carlsbad, CA) were cultured and seeded at 15 000 cells/well in black solid-bottom 96-well plates (Cat#353376, BD Biosciences, Franklin Lakes, NJ). The cells were washed and growth-arrested with serum-free MCM media (ScienCell Research, Carlsbad, CA). After 24 h, the cells were stimulated with serial dilutions of PDGF-BB for 4 h at 37 °C. DNA synthesis was determined during the last 16 h using a 5-bromo-2′-deoxyuridine (BrdU) incorporation assay according to the manufacturer's instructions (Roche, Mannheim, Germany). The following day, the cells were fixed and assayed for BrdU incorporation according to the manufacturer's protocol.

The Schild analysis was performed as previously described.[52] Briefly, a constant amount of MOR8457-hIgG1 or PDGFRβ-ECD-hIgG1 was mixed with samples of serially diluted PDGF-BB before adding to the cells. The EC_{50} value of PDGF-BB measured in the absence and presence of antagonists was used to calculate the dose ratio (DR). A series of log (DR-1) values

Table 3. Binding Affinity and Specificity of MOR8457 and PDGFRβ-ECD-hIgG1 Fusion Proteins to Different PDGF Family Members Determined by Surface Plasmon Resonance

	MOR8457-hIgG1			MOR8457-mIgG1			PDGFRβ-ECD-hIgG1[b]		
isoform	k_a (M^{-1} s^{-1})	kd (s^{-1})	K_D (pM)	k_a (M^{-1} s^{-1})	kd (s^{-1})	K_D (pM)	k_a ($M^{-1}s^{-1}$)	kd (s^{-1})	K_D (pM)
hBB	1.27×10^7	3.62×10^{-4}	28	1.12×10^7	NA[a]	<10	3×10^7	4×10^{-4}	13 ± 5
mBB	2.95×10^7	2.93×10^{-4}	10	2.48×10^7	NA[a]	<10	6.3×10^7	1.1×10^{-4}	2 ± 1
rBB	1.77×10^7	4.47×10^{-4}	25	1.42×10^7	NA[a]	<10	4×10^7	1.4×10^{-4}	4 ± 1
hAB	0.65×10^7	4.50×10^{-4}	69	0.59×10^7	NA[a]	<10	no binding		
hDD	no binding			no binding			3×10^7	4.2×10^{-4}	16 ± 1

[a]K_{off} could not be accurately measured (below instrument limit). [b]Data for PDGFRβ-ECD-hIgG1 werethe average of two independent experiments.

DOI: 10.1021/bi5015425
Biochemistry 2015, 54, 1918−1929

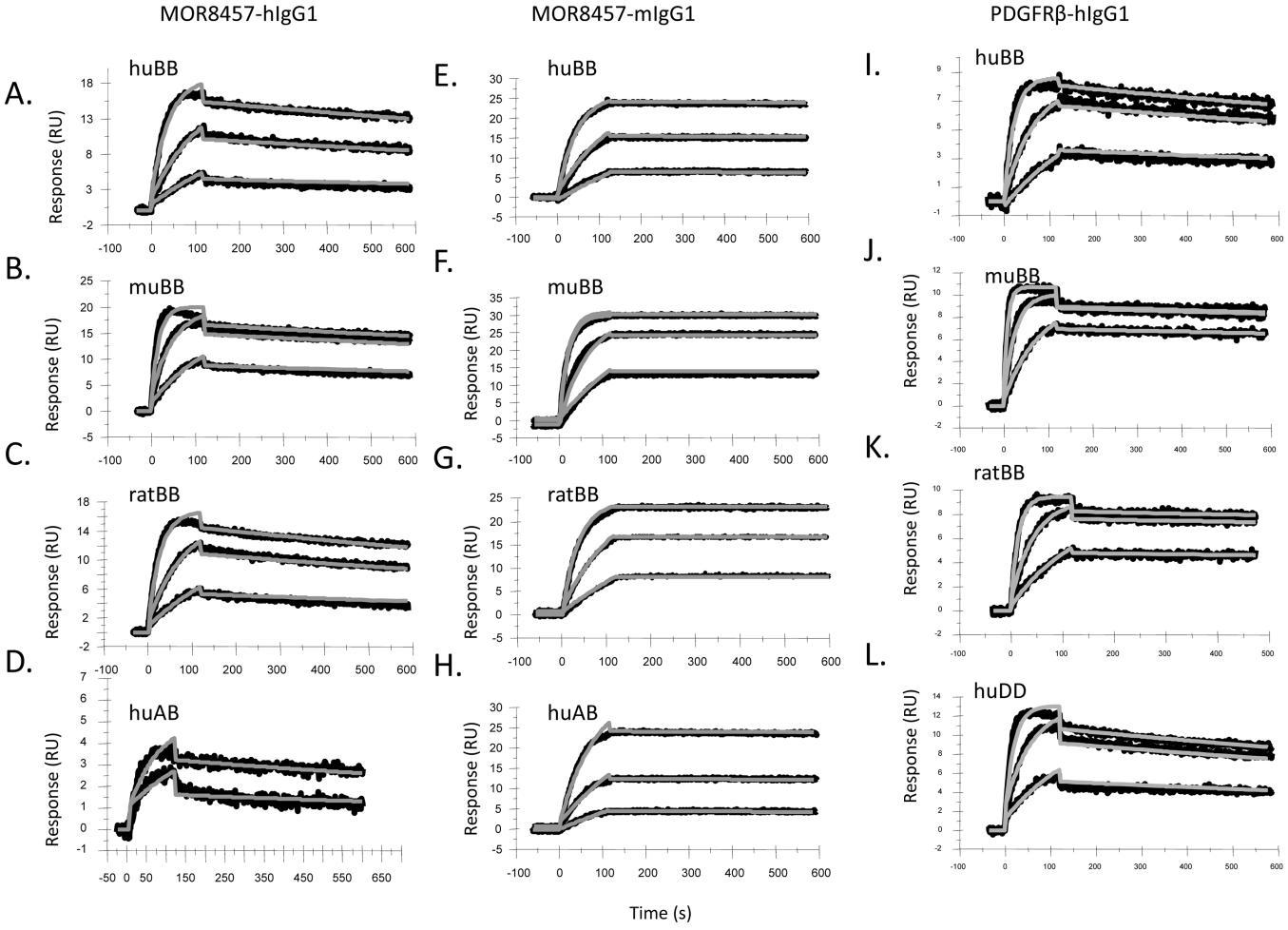

Figure 1. Sensorgrams of binding kinetics of MOR8457 and PDGFRβ-ECD-hIgG1 to different PDGFs. MOR8457-hIgG1 (A–D), MOR8457-mIgG1 (E–H), or PDGFRβ-ECD-hIgG1 (I–L) were captured by antihuman (A–D, I–L) or antimouse (E–H) IgG antibodies immobilized on CM5 sensor chips. Different concentrations of each PDGF protein (0.25, 0.5, and 1 nM) were injected over the surface with the exception that only 0.5 nM and 1 nm of human PDGF-AB was injected to the surface of MOR8457-hIgG1 (D). The determined binding affinities are listed in Table 3. MOR8457-hIgG1 and MOR8457-mIgG1 showed low pM binding affinities to human, mouse, and rat PDGF-BB, which were comparable with those of PDGFRβ-ECD-hIgG1 binding. MOR8457 bound to PDGF-AB but not PDGF-DD, in contrast, PDGFRβ-ECD-hIgG1 bound to PDGF-DD but not PDGF-AB. MOR8457-hIgG1 (A–D) and MOR8457-mIgG1 (E–H) showed a similar on-rate to each PDGF protein; however, MOR8457-mIgG1 (E–H) showed slower off-rates than MOR8457-hIgG1. The off-rates of MOR8457-mIgG1 were outside the limit of the instrument and estimate the K_D to be less than 10 pM.

for a series of log [B] antagonist concentrations were plotted and the pA_2 value determined by extrapolation.

RESULTS

Identification and Functional Properties of MOR8457. MOR8457 was identified by screening a MorphoSys HuCAL GOLD phagemid library[53] for Fabs that specifically bound and neutralized PDGF-BB. The VH domains of the MOR8457 Fab were grafted onto mouse wild type IgG1 and human Fc effector null IgG1 heavy chain constant domains, to generate MOR8457-mIgG1 and MOR8457-hIgG1 respectively. The VL domains were similarly grafted on to orthologous kappa light chain backbones.

The binding properties of MOR8457-mIgG1 and MOR8457-hIgG1 for PDGF were compared with a recombinantly expressed PDGFRβ-ECD-hIgG1 Fc fusion protein by surface plasmon resonance by BIAcore (Table 3 and Figure 1). The binding affinities of MOR8457 and PDGFRβ-ECD-hIgG1 for human and rodent PDGF-BB were highly comparable. In contrast, the binding of MOR8457 for PDGF-DD was negligible compared with PDGFRβ-ECD-hIgG1 and MOR8457 was able to bind to human PDGF-AB (Table 3). The functional properties of MOR8457 were determined by evaluating the effect of increasing concentrations of MOR8457-hIgG1 and PDGFRβ-ECD-IgG1 on PDGF-BB induced proliferation of human renal mesangial cells. Both MOR8457-hIgG1 and PDGFRβ-ECD-hIgG1 induced a characteristic rightward shift in the PDGF-BB concentration response curve, indicative of competitive antagonism (Figure 2). The resultant Schild analysis indicated that MOR8457-hIgG1 and PDGFRβ-ECD-hIgG1 were able to inhibit cell proliferation with K_B values of 29 and 55 pM respectively (Figure 2).

Binding Properties and Stoichiometry of Binding of MOR8457. While the Schild analysis suggested that MOR8457-hIgG1 and PDGFRβ-ECD-hIgG1 had a similar mode of action, the pattern of binding to different PDGFs suggested that the binding modes of MOR8457 and PDGFRβ-ECD-hIgG1 were different. To explore this in more detail, the stoichiometry of binding was assessed biophysically by surface plasmon resonance using BIAcore. For this, MOR8457-mIgG1

DOI: 10.1021/bi5015425
Biochemistry 2015, 54, 1918–1929

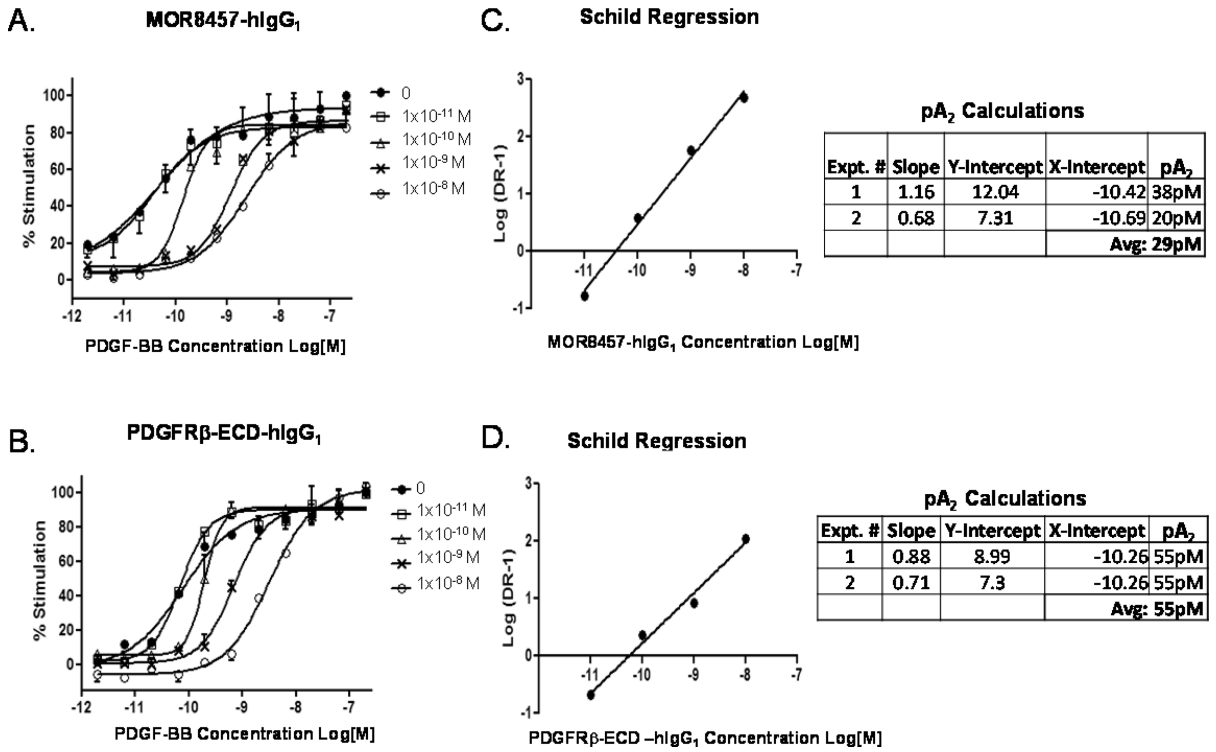

Figure 2. Concentration-dependent, competitive inhibition of human mesangial cell proliferation by MOR8457-hIgG1 and PDGFRβ-ECD-hIgG1. The effects of increasing concentrations of MOR8457-hIgG1 (0.01, 0.1, 1, and 10 nM) (A) or PDGFRβ-ECD-hIgG1 (B) on the concentration response curve of PDGF-BB were tested on human mesangial cell proliferation. Antagonists were mixed with PDGF-BB and incubated for 2.5 h at 25 °C before adding to the cells. Cell proliferation assay was performed as described in Experimental Procedures. Curves shifted to the right with the increased concentration of MOR8457-hIgG1 or PDGFRβ-ECD-hIgG1. The extent of the inhibition was surmountable at high concentrations of PDGF-BB, a feature of competitive and reversible inhibition. Schild analysis was performed. Schild regressions of MOR8457-hIgG1 (C) or PDGFRβ-ECD-hIgG1 (D) are represented. The average calculated pA_2 from two independent experiments was 29 pM for MOR8457-hIgG1 and 55 pM for PDGFRβ-ECD-hIgG1. The graphs are a representative from two independent experiments.

was first immobilized on the CM5 chip and human PDGF-BB bound to form a complex. This complex was then further interrogated by further injection of either MOR8457-hIgG1 or PDGFRβ-ECD-hIgG1. MOR8457-hIgG1 was able to bind the MOR8457-mIgG1/PDGF-BB complex, but PDGFRβ-ECD-hIgG1 was not (Figure 3A). These data suggested that one PDGF-BB dimer binds to two MOR8457 antibody molecules, in contrast to PDGFRβ, where the PDGF binding site is formed from chains in adjacent receptor molecules.[54] To confirm whether the binding of PDGF-BB to MOR8457 induced a conformational change in PDGF-BB which rendered the ligand incapable of binding PDGFRβ, a single chain version of PDGFRβ-ECD-hIgG1, termed Fab-hIgG1-PDGFR(D1-D3), was tested for binding on preassembled MOR8457-hIgG1-PDGF-BB. This single chain version bound to PDGF-BB with less, but measurable, affinity than PDGFRβ-ECD-hIgG1 (K_D 528 pM (Figure 3C) c.f 13.5 pM (Table 2)), but this variant had no significant binding affinity for the MOR8457-hIgG1/PDGF-BB complex indicating that MOR8457 either sterically blocks the binding of PDGF-BB to PDGFRβ or stabilizes a nonpermissive conformation in the second PDGF-B chain (Figure 3B).

Structure of MOR8457-PDGF-BB Complex. MOR8457-PDGF-BB crystals gave synchrotron diffraction to 2.3 Å (Table 1, Supplemental Figure 1, Supporting Information). The overall architecture of the complex reveals a two-site binding mode, in which one PDGF-BB ligand is trapped between two MOR8457 Fab molecules (Figure 4). The structure of PDGF-BB in this complex is similar to the previously reported structures[54,55] and has a covalently linked dimer structure, with an anti-parallel β-sheet at the center and three loops at the dimer far ends, L1, L2, and L3. The binding of MOR8457 to each of these ends separates the C-termini of the two Fabs by as much as 190 Å, giving an elongated geometry to the complex (Figure 4). This imposes spatial constraints on binding partners, and, in agreement with the BIAcore studies (Figure 3), confirmed that the binding stoichiometry of the MOR8457-PDGF-BB complex is 2:1; i.e., two molecules of MOR8457 bind to each PDGF-BB.

Antigen–Antibody Interface and Its Charge Complementarity. The binding of MOR8457 follows the approximate 2-fold symmetry of the PDGF-BB-dimer, creating two interacting surfaces and hence the two symmetrical epitopes on the ligand surface. As both binding surfaces involve similar interactions, the analysis described below will refer to the epitope that involves the antibody chains H and L and the ligand protomers C and D.

The CDRs on the surface of the antibody create a wide cleft, roughly the shape of a triangle, harboring the three PDGF-BB loops L1, L2, and L3 (Figure 4). A total of 39 amino acid residues participate in the interface, based on the fact that they are less than 4 Å apart (Table 2), with 17 residues coming from PDGF-BB and 22 residues from the MOR8457 Fab. The PDGF-BB residues that appear to be essential for binding to the antibody are contributed by both PDGF-BB chains, with 87% of the interactions coming from L1 and L3 of one chain,

DOI: 10.1021/bi5015425
Biochemistry 2015, 54, 1918–1929

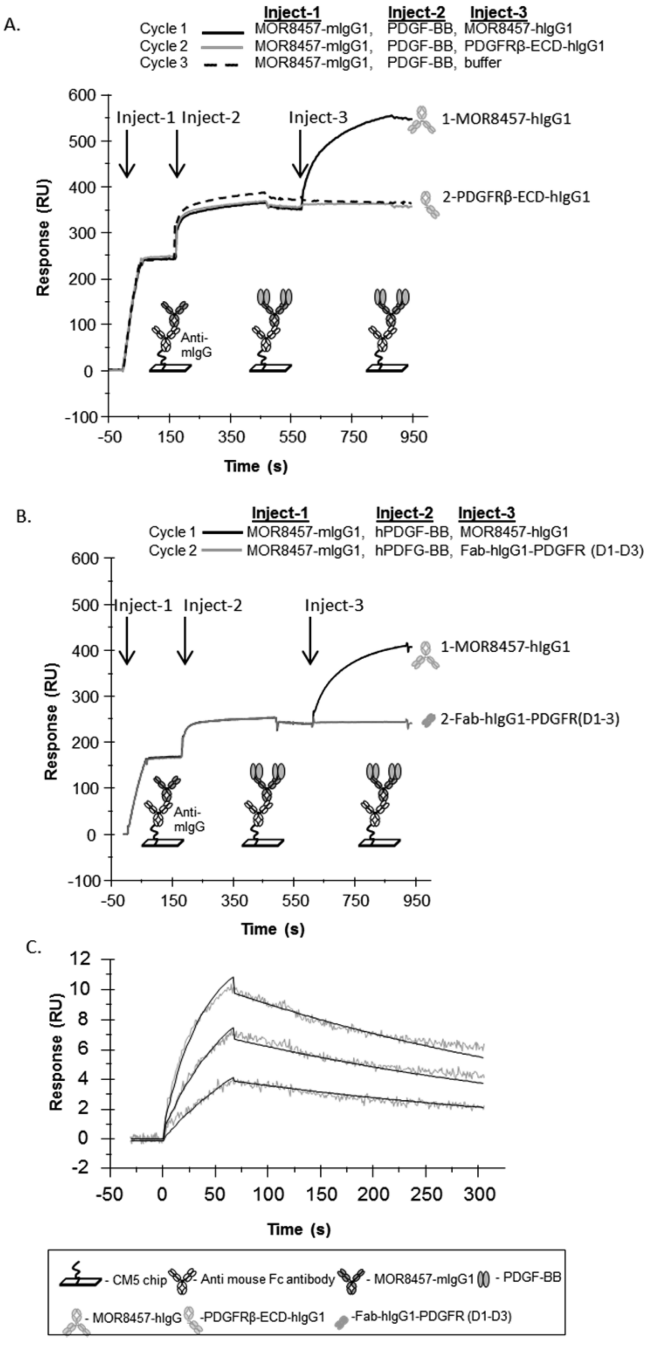

Figure 3. Delineation of binding mode of action of MOR8457 to PDGF-BB by surface plasmon resonance using BIAcore. MOR8457-mIgG1 was captured via antimouse IgG immobilized onto a CM5 sensor chip (Inject 1). Human PDGF-BB was injected to reach the surface saturation (Inject 2), followed by injection of (A) MOR8457-hIgG1 (Cycle 1, Inject 3, black line), or PDGFRβ-ECD-hIgG1 (Cycle 2, Inject 3, gray line), or buffer (Cycle 3, Inject 3, dash line), or (B) MOR8457-hIgG1(Cycle 1, black line) or Fab-hIgG1-PDGFR(D1-D3) (Cycle 2, gray line). (C) shows that Fab-hIgG1-PDGFR(D1-D3), can bind free PDGF-BB with a K_D value of 528 ± 28 pM. Neither PDGFRβ-ECD-hIgG1 (A) nor Fab-hIgG1-PDGFR(D1-D3) (B) were able to bind to preassembled MOR8457-mIgG1/PDGF-BB complex on the chip suggesting that the MOR8457 binding sites competed with the PDGFRβ binding sites. In contrast, MOR8457-hIgG1 bound to preassembled MOR8457-mIgG1/PDGF-BB complex suggesting that one PDGF-BB dimer bound to two MOR8457 molecules as illustrated in the diagram. Data are one representative of at least two independent experiments.

with the largest contribution from L3, and the remaining 13% coming from L2 of the other chain. Residues essential for MOR8457 binding to the antigen are contributed by all CDRs, except CDR-H1, and with the largest contribution coming from CDR-H3 (Table 2).

Numerous favorable interactions stabilize this complex formation, including hydrophobic and polar aromatic ring interactions, and 14 hydrogen bonds. The most striking feature of the interface is the high charge complementarity between the two binding partners: one with the CDR surface mainly negatively charged (Figure 5A) and the other positively charged (Figure 5B), in contrast to the PDGFRβ-PDGF-BB interface.[54]

Structural Basis for Inhibition of PDGFRβ Binding. The BIAcore studies indicated that the MOR8457 bound conformation of PDGF-BB may be different from the PDGFRβ-bound complex as MOR8457-PDGF-BB was able to bind MOR8457, but not PDGFRβ (Figure 3B). We evaluated the structural basis for this difference and noted that, as well as blocking PDGFRβ activity by occupying a similar binding site on PDGF-BB, MOR8457 had an effect on ligand conformation. The most notable change in PDGF-BB upon MOR8457 binding is the pronounced bending of the dimer compared with the more flattened forms seen in its free and receptor bound states (Figure 6A). Importantly, the resulting bend in the structure of PDGF-BB sterically obscures the PDGFRβ-binding epitope. The crystal structures of PDGF-BB have been previously reported alone,[55] in complex with the PDGFRβ[54] or in complex with a synthetic aptamer.[56] In the unligated state, the L1 loop is completely disordered, while the structures of L2 and L3 fall within the range of conformations observed in the ligand-bound states. Superimposing the structure of the PDGF-BB molecule as observed in our structure (black) onto the conformations seen in the unbound state (green), in bound states with PDGFRβ (red) and aptamer (blue) indicated considerable displacement (bend and twist) in the PDGF-B structure relative to one another (Figure 6B,C). The displacements result in root-mean-square deviation (r.m.s.d.) values of 0.59 Å (for 131 Cα-pairs, black-green), 0.74 Å (for 134 Cα-pairs, black-red), and 1.62 Å (for 147 Cα-pairs, black-blue) for each of the structures, respectively. The differences in r.m.s.d. are due mainly to variations in L3 loop orientations relative to the PDGF-BB 2-fold axis, with the highest deviations at the tip of the loop, the Cα-position of Arg 79 (Figure 6C). Calculating the displacement of the PDGF-BB Arg 79 Cα atom in the MOR8457 structure compared with PDGF-BB alone and in its PDGFRβ bound state indicated a 21.8° bending angle and 10.5 Å bending distance difference in the PDGF-BB structure between MOR8457 and PDGFRβ bound states (Figure 6C). Thus, the effect of MOR8457 inhibition could be both blocking the PDGF-BB binding directly and stabilizing a PDGF-BB conformation that is incompatible with the receptor binding. These structural observations were entirely consistent with the BIAcore observations (Figure 3).

MOR8457 Specificity. The observed MOR8457-PDGF-BB complex structure and its comparison with the PDGFRβ-bound PDGF-BB[54] suggested that MOR8457 antagonizes PDGFRβ by directly competing with the receptor for the same binding determinants. Indeed, superposition of the MOR8457-PDGF-BB complex and the PDGF-BB-PDGFRβ complex reveals that the antibody and the receptor compete for the same binding locus of PDGF-BB, but in different binding modes (Figure 7). The two overlapping positions are both centered at the L3

DOI: 10.1021/bi5015425
Biochemistry 2015, 54, 1918−1929

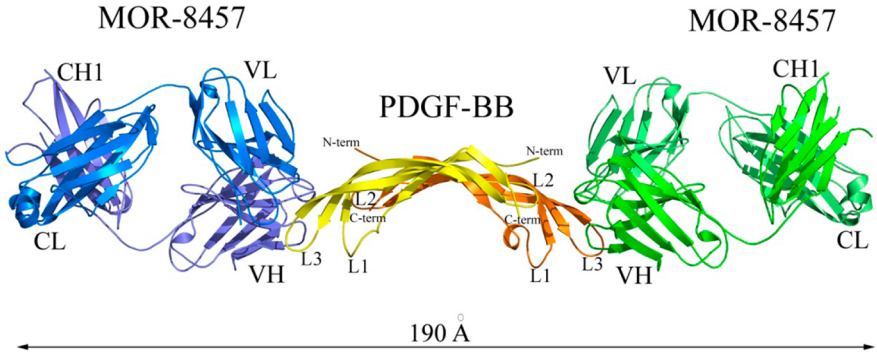

Figure 4. Structure and geometry of the MOR8457-PDGF-BB complex. The ligand dimer bound to two Fab molecules is shown in yellow and orange ribbons, and the Fabs in blue and green ribbons. L1, L2, and L3 are the three loops on each of the ligand chains that are part of the epitope recognized by MOR8457. The value of 190 Å indicates the distance between the C-terminal ends of the two Fab molecules.

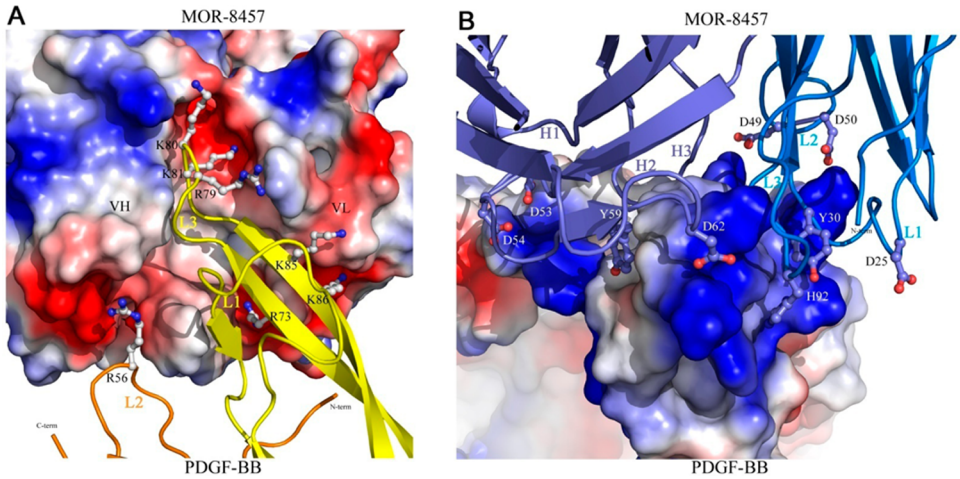

Figure 5. MOR8457-PDGF-BB interface. Two representations of the interaction illustrating its charge complementarity. (A) Electrostatic surface potential of the MOR8457 paratope, with the PDGF-BB epitope in yellow and orange ribbons. (B) Electrostatic surface potential of the PDGF-BB epitope, with the MOR8457 paratope in blue ribbons. Both surfaces are colored according to electrostatic potential ranging from most negative −60 kT/e (red) to most positive +60 kT/e (blue), where k is the Boltzmann constant and T is the absolute temperature. The acidic and the corresponding basic residues that contribute to the charge complementary are shown as a ball-and-stick model.

loop, but tilted at a right angle with respect to each other. These differences in the receptor and antibody positions may account, as discussed in detail below, for the narrow selectivity of MOR8457 for the PDGF-BB isoform and for the ability of PDGFRβ to bind both PDGF-BB and PDGF-DD isoforms.

DISCUSSION

The family of platelet-derived growth factors (PDGF-A, -B, -C, and -D) plays an important role in embryonic development, vascular and tissue remodeling as well as the proliferation of endothelial cells, fibroblasts, and smooth muscle cells. The ligands function as highly homologous disulfide dimers, binding to specific PDGF receptor pairs to facilitate dimerization and tyrosine kinase activity. The role of the pathway in human health and disease has been exemplified by numerous expression studies and experimental assessments. Of these, PDGF-BB has been demonstrated to be unregulated in number of malignant and fibrotic conditions.[10,11,13,57−59] These observations have also been followed up experimentally with small molecule tyrosine kinase inhibitors, antisense, aptamers, and blocking antibodies[17,28,29,31,32,34,36] in a number of different preclinical fibrosis models, indicating specific PDGF-B blockade may have therapeutic benefit. Consequently, there is tremendous interest in selective PDGF-B approaches, and the development of such therapies would benefit from detailed structural analyses to help support confidence in rationale and PK/PD modeling.[54,60]

Here we have described the identification and pharmacological characterization of MOR8457, a highly potent and selective blocking PDGF-BB monoclonal antibody. In binding and functional assays measuring the effect of MOR8457 on PDGF-BB-induced cell proliferation, MOR8457 was demonstrated to bind reversibly and competitively (Figure 2 and Table 3). Supporting these functional credentials, preliminary efficacy studies have further indicated that MOR8457-mIgG1 dose dependently blocks hepatic stellate cell proliferation and liver fibrosis in a rodent model.[60] Taken together, these data support the therapeutic rationale of utilizing MOR8457 for liver fibrosis as well as other fibrotic conditions.

We extended these pharmacological and biophysical assessments to also describe the structure of the MOR8457-PDGF-BB interaction, its stoichiometry, the specificity, and compared with other PDGF-BB structures, the difference in conformation that PDGF-BB adopts on MOR8457 binding to obscure PDGFRβ ligation. Both biophysical characterization and structural determination have indicated that two MOR8457 molecules bind to one PDGF-BB, with high affinity; however, the binding of one MOR8457 molecule appears to be sufficient

DOI: 10.1021/bi5015425
Biochemistry 2015, 54, 1918−1929

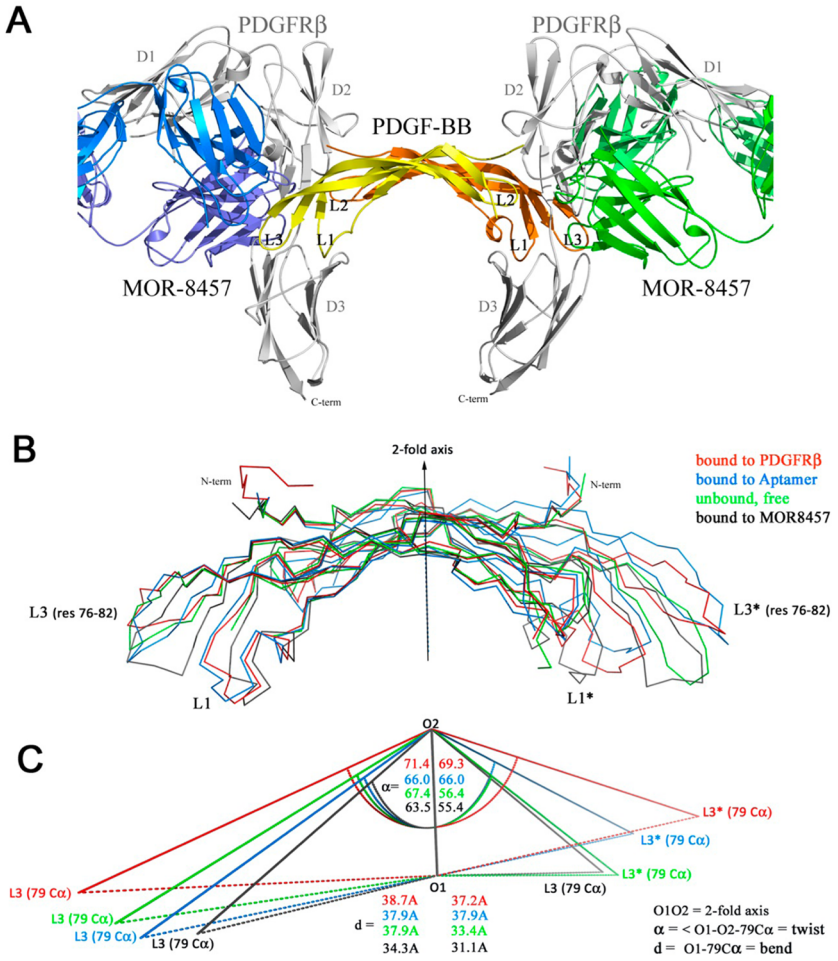

Figure 6. Comparison of the MOR8457 bound PDGF-BB dimer with existing PDGF-BB structures. (A) Ribbon diagram showing overlay of the MOR8457-PDGF-BB complex (blue, green, and yellow-orange, respectively) on top of the PDGFRβ -PDGF-BB complex (PDGFRβ in gray and PDGF-BB omitted for clarity). The superposition, based solely on the PDGF-BB dimer, illustrates that MOR8457 uses the same L1, L2, and L3 binding determinants on PDGF-BB as PDGFRβ. (B) Cα trace diagram showing overlay of the PDGF-BB structures in the MOR-8457 bound form (black, pdb ID = 4QCI), the receptor bound form (red, pdb ID = 3MJG), the aptamer-bound form (blue, pdb ID = 4HQX), and the free, unliganded form (green, pdb ID = 1PDG). In each structure the PDGF-BB dimer follows an approximate 2-fold rotational symmetry, except for the aptamer-bound PDGF-BB, where a perfect (crystallographic) 2-fold axis, shown as the vertical line, relates the two PDGF-B subunits. The overall similarity with the previously reported structures is apparent, as is the substantial but localized changes in the loop regions for each of the subunits. (C) The displacement of loop 3 calculated as bend d (angstroms) and a bending angle, twist α (degree) relative to its respective positions in the other structures. The same coloring scheme is used as in (B).

to block binding to PDGFRβ from these studies (Figure 3). Complex formation appears to be strongly driven by electrostatic steering (Figure 5), and both the steric determinants in the longer L3 loop of PDGF-D and electrostatic surfaces contribute to the exquisite selectivity for PDGF-BB over the related PDGF-DD. Various studies have shown that a strong electrostatic surface complementarity in protein−protein interactions enhances the association rate constant by forming of a transient encounter complex before the final high affinity complex is formed.[61] In agreement with this concept, the association rate constants (K_{on}) between MOR8457 and PDGF-BB were found to be fast from the binding kinetics measured by surface plasmon resonance (Table 3).

There is remarkable similarity in the structure of the central β-strands of the free PDGF-BB, PDGFRβ-bound PDGF-BB, and the MOR8457 bound PDGF-BB (Figure 7B). However, the BIAcore biophysical characterization suggested that occupying one binding site on PDGF-BB by MOR8457 was sufficient to block PDGFRβ binding to the other half of the ligand dimer. A number of crystal structures of PDGF-BB have been previously reported either alone,[55] in complex with PDGFRβ[54] or a synthetic aptamer.[56] The overall folding pattern of PDGF-BB in these structures is maintained, but the conformation of the residues located in three loop regions L1, L2, and L3 differs substantially for each of the two subunits (Figure 6). This is not surprising, as growth factor binding and function are primarily driven through interactions at these loops (Figure 6A). In the unligated state, the L1 loop is completely disordered, while the structures of L2 and L3 fall within the range of conformations observed in the ligand-bound states. Superimposing the structures of PDGF-BB around the Cα-position of Arg 79 in these different complexes indicated a marked bending and twisting of the ligand between these different states (Figure 6B,C). For MOR8457 bound PDGF-BB, the displacement of the PDGF-BB Arg 79 Cα atom was a −21.8° difference in the bending angle and −10.5 Å difference in the bending distance difference compared with PDGF-BB in its PDGFRβ bound state. This significant

DOI: 10.1021/bi5015425
Biochemistry 2015, 54, 1918−1929

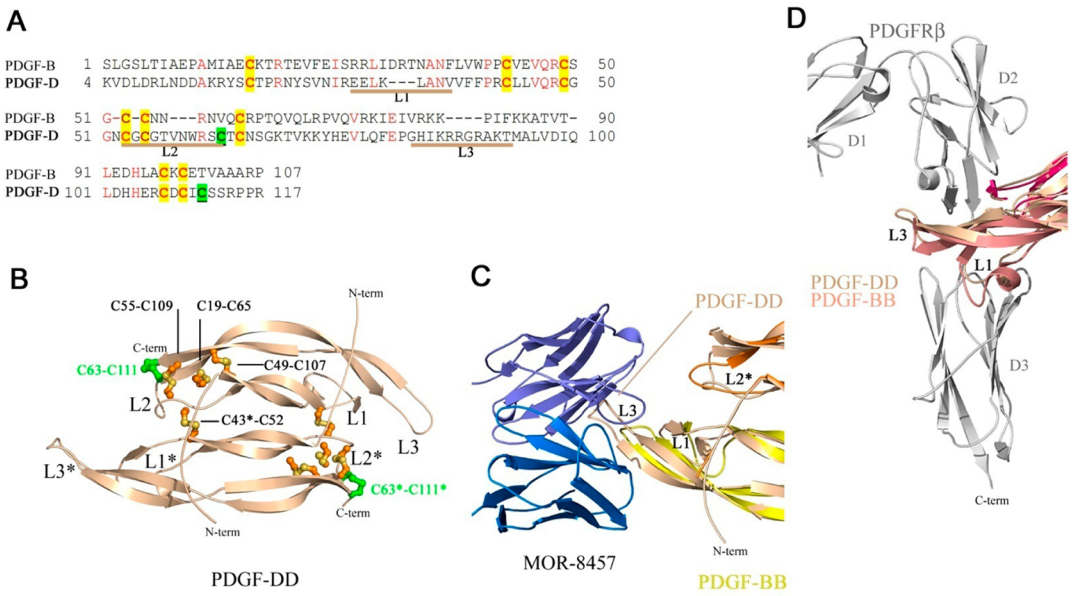

Figure 7. Structure-based homology modeling of PDGF-DD and comparison with existing PDGF-BB structures. (A) Amino-acid sequence alignment between PDGF-B and the growth factor domain of PDGF-D, the two sharing ~25% sequence identity. Alignment was performed with Clustal-W[49] and manually adjusted to satisfy cysteine pairs that form disulfides in PDGF-BB. Residues that are strongly conserved between PDGF-B and PDGF-D are painted in red, with the conserved cysteines highlighted in yellow and the two extra cysteines in PDGF-D highlighted in green. The PDGFRβ and MOR8457 binding elements on PDGF-B, L1, L2 and L3, are underlined and labeled. (B) Ribbons model of the PDGF-DD dimer. The model was built with Modeler[50] using the structure of PDGF-BB as a homologous crystal template. Dimer disulfides are shown as a ball-and-stick model, with eight conserved disulfides in orange-yellow and two new disulfides in green. Asterisks denote ligand dimer partner. (C) Overlay of the PDGF-DD dimer (wheat) on top of the PDGF-BB dimer (yellow-orange) bound to MOR8457 (blue). The view illustrates that the longer loop L3 insertion in PDGF-D would create steric hindrance, thus a barrier to MOR8457 binding. (D) Overlay of the PDGF-DD dimer (wheat) on top of the PDGF-BB dimer (yellow-orange) bound to PDGFRβ (gray). The view illustrates that the longer loop L3 insertion in PDGF-D would not introduce steric hindrance to PDGFRβ binding.

distortion in PDGF-BB structure observed in the MOR8457 bound state we believe strongly supports the biophysical data and the hypothesis that MOR8457 binding to PDGF-BB both directly impairs PDGFRβ binding and introduces sufficient steric constraint in PDGF-BB to indirectly impair PDGFRβ binding as well. How does the binding of one antibody binding site to the PDGF-BB dimer appear to be sufficient to prevent receptor binding to the other site is an important consideration. If one considers that there is considerable conformational flexibility in the ligand, then one possibility is that when MOR8457 binds to one monomer of the PDGF-BB dimer, it proceeds through a co-operative change in conformation across the entire dimeric structure, communicating this binding event to the second symmetrical binding site. Such co-operative changes could provide synchronized conformational sampling enhanced by the intrinsic disulfide tether between the two monomers, suggesting that the two binding sites in the PDGF-BB dimer are in fact a pair of coupled and coregulated receptor recognition sites. By locking out a nonreceptor competent conformation on one monomer the antibody effectively locks out the corresponding conformation on the other monomer. These observations complement others, especially in the IL-6 and HER-2 space,[62,63] which indicates that there is remarkable conformational freedom in antibody–ligand interactions, in the antibody as well as the target protein, and that in the process of antibody selection it is possible to select an antibody, illustrated here by MOR8457, that is able to trap a PDGF-BB conformation that is not permissive for receptor ligand binding.

With the aid of (1) a structure-based sequence alignment between PDGF-B and the growth factor domain of PDGF-D (Figure 7A) and (2) homology-based 3D-models of PDGF-DD (Figure 7B) and of PDGFRβ-PDGF-DD complex (Figure 7D), we have concluded that the mode of interaction with the L3 loop is probably the key factor that defines the difference in their binding capacities to PDGF-DD (Figure 7C,D).

While this is the first structural analysis of PDGF-B blocking antibody bound to PDGF-BB, the structural and biophysical insights have increased our knowledge of the nature of PDGFRβ agonism and antagonism that might be important in the development of selective modulators of the PDGFRβ axis, for instance, in the development of bispecific mAbs where inhibition of activity is conferred by the binding of one Fab arm. Furthermore, that the binding of one MOR8457 molecule is sufficient to fully antagonize the effects of PDGF-BB on PDGFRβ will be important in the development of a PK/PD model to help facilitate the selection of doses and dosing frequency for experimental evaluations.[60]

■ ASSOCIATED CONTENT

Ⓢ Supporting Information

An example of the final electron density map is shown in Supplemental Figure 1. This material is available free of charge via the Internet at http://pubs.acs.org.

■ AUTHOR INFORMATION

Corresponding Author

*E-mail: nick.pullen@pfizer.com.

Author Contributions

#These authors (J.K. and L.M.) contributed equally.

DOI: 10.1021/bi5015425
Biochemistry 2015, 54, 1918–1929

Funding

This research work was funded by Pfizer Global Research & Development.

Notes

The authors declare the following competing financial interest(s): MOR8457 was identified as a part of a Pfizer funded research collaboration. JK, LM, JB, MC, SO, TI, MT, ERL, ZY and NP are current employees of Pfizer.

■ ACKNOWLEDGMENTS

The authors are extremely grateful for the guidance and input from Simeon Ramsey on the design of the Schild analysis studies, to Lisa Collins and Karl Malakian for their contribution to protein expression work, and Kristine Svenson for supporting the crystal growth work.

■ ABBREVIATIONS

ECD, extracellular domain; ELISA, enzyme-linked immunosorbant assay; PDGF, platelet-derived growth factor; PDGFRβ, PDGF receptor-β; IgG, immunoglobulin; IPTG, isopropyl β-D-thiogalactoside; PK/PD, pharmacokinetic/pharmacodynamic

■ REFERENCES

(1) Trojanowska, M. (2008) Role of PDGF in fibrotic diseases and systemic sclerosis. *Rheumatology (Oxford, England) 47* (Suppl. 5), v2–4.

(2) Ostendorf, T., Eitner, F., and Floege, J. (2012) The PDGF family in renal fibrosis. *Pediatr. Nephrol.(Berlin, Germany) 27*, 1041–1050.

(3) Andrae, J., Gallini, R., and Betsholtz, C. (2008) Role of platelet-derived growth factors in physiology and medicine. *Genes Dev. 22*, 1276–1312.

(4) Boor, P., Eitner, F., Cohen, C. D., Lindenmeyer, M. T., Consortium, E., Mertens, P. R., Ostendorf, T., and Floege, J. (2009) Patients with IgA nephropathy exhibit high systemic PDGF-DD levels. *Nephrol., Dial., Transplant. 24*, 2755–2762.

(5) Eitner, F., Ostendorf, T., Kretzler, M., Cohen, C. D., Eriksson, U., Grone, H. J., Floege, J., and Consortium, E. (2003) PDGF-C expression in the developing and normal adult human kidney and in glomerular diseases. *J. Am. Soc. Nephrol. 14*, 1145–1153.

(6) Yoshimura, A., Gordon, K., Alpers, C. E., Floege, J., Pritzl, P., Ross, R., Couser, W. G., Bowen-Pope, D. F., and Johnson, R. J. (1991) Demonstration of PDGF B-chain mRNA in glomeruli in mesangial proliferative nephritis by in situ hybridization. *Kidney Int. 40*, 470–476.

(7) Nakamura, T., Ebihara, I., Nagaoka, I., Tomino, Y., and Koide, H. (1992) Renal platelet-derived growth factor gene expression in NZB/W F1 mice with lupus and ddY mice with IgA nephropathy. *Clin. Immunol. Immunopathol. 63*, 173–181.

(8) Langham, R. G., Kelly, D. J., Maguire, J., Dowling, J. P., Gilbert, R. E., and Thomson, N. M. (2003) Over-expression of platelet-derived growth factor in human diabetic nephropathy. *Nephrol., Dial., Transplant. 18*, 1392–1396.

(9) Iida, H., Seifert, R., Alpers, C. E., Gronwald, R. G., Phillips, P. E., Pritzl, P., Gordon, K., Gown, A. M., Ross, R., Bowen-Pope, D. F., et al. (1991) Platelet-derived growth factor (PDGF) and PDGF receptor are induced in mesangial proliferative nephritis in the rat. *Proc. Natl. Acad. Sci. U.S.A. 88*, 6560–6564.

(10) Bessa, S. S., Hussein, T. A., Morad, M. A., and Amer, A. M. (2012) Urinary platelet-derived growth factor-BB as an early marker of nephropathy in patients with type 2 diabetes: an Egyptian study. *Ren. Fail. 34*, 670–675.

(11) Wang, Q. Y., Guan, Q. H., and Chen, F. Q. (2009) The changes of platelet-derived growth factor-BB (PDGF-BB) in T2DM and its clinical significance for early diagnosis of diabetic nephropathy. *Diabetes Res. Clin. Pract. 85*, 166–170.

(12) Changsirikulchai, S., Hudkins, K. L., Goodpaster, T. A., Volpone, J., Topouzis, S., Gilbertson, D. G., and Alpers, C. E. (2002) Platelet-derived growth factor-D expression in developing and mature human kidneys. *Kidney Int. 62*, 2043–2054.

(13) Matsuda, M., Shikata, K., Makino, H., Sugimoto, H., Ota, K., Akiyama, K., Hirata, K., and Ota, Z. (1997) Gene expression of PDGF and PDGF receptor in various forms of glomerulonephritis. *Am. J. Nephrol. 17*, 25–31.

(14) Naito, T., Nitta, K., Ozu, H., Tsuchiya, K., Matsugami, K., Honda, K., Yumura, W., and Nihei, H. (1997) Clinical assessment of the significance of platelet-derived growth factor in patients with immunoglobulin A nephropathy. *J. Lab. Clin. Med. 130*, 63–68.

(15) Terada, Y., Yamada, T., Nakashima, O., Sasaki, S., Nonoguchi, H., Tomita, K., and Marumo, F. (1997) Expression of PDGF and PDGF receptor mRNA in glomeruli in IgA nephropathy. *J. Am. Soc. Nephrol. 8*, 817–819.

(16) Uehara, G., Suzuki, D., Toyoda, M., Umezono, T., and Sakai, H. (2004) Glomerular expression of platelet-derived growth factor (PDGF)-A, -B chain and PDGF receptor-alpha, -beta in human diabetic nephropathy. *Clin. Exp. Nephrol. 8*, 36–42.

(17) Floege, J., Eng, E., Young, B. A., Alpers, C. E., Barrett, T. B., Bowen-Pope, D. F., and Johnson, R. J. (1993) Infusion of platelet-derived growth factor or basic fibroblast growth factor induces selective glomerular mesangial cell proliferation and matrix accumulation in rats. *J. Clin. Invest. 92*, 2952–2962.

(18) Shultz, P. J., DiCorleto, P. E., Silver, B. J., and Abboud, H. E. (1988) Mesangial cells express PDGF mRNAs and proliferate in response to PDGF. *Am. J. Physiol. 255*, F674–684.

(19) Silver, B. J., Jaffer, F. E., and Abboud, H. E. (1989) Platelet-derived growth factor synthesis in mesangial cells: induction by multiple peptide mitogens. *Proc. Natl. Acad. Sci. U.S.A. 86*, 1056–1060.

(20) Wallmon, A., Fellstrom, B., Larsson, R., Floege, J., Topley, N., and Ljunghall, S. (1993) PDGF-BB, but not PDGF-AA, stimulates calcium mobilization, activation of calcium channels and cell proliferation in cultured rat mesangial cells. *Exp. Nephrol. 1*, 238–244.

(21) Floege, J., Topley, N., and Resch, K. (1991) Regulation of mesangial cell proliferation. *Am. J. Kidney Dis. 17*, 673–676.

(22) Tang, W. W., Ulich, T. R., Lacey, D. L., Hill, D. C., Qi, M., Kaufman, S. A., Van, G. Y., Tarpley, J. E., and Yee, J. S. (1996) Platelet-derived growth factor-BB induces renal tubulointerstitial myofibroblast formation and tubulointerstitial fibrosis. *Am. J. Pathol. 148*, 1169–1180.

(23) Ishizaka, N., Matsuzaki, G., Saito, K., Noiri, E., Mori, I., and Nagai, R. (2006) Expression and localization of PDGF-B, PDGF-D, and PDGF receptor in the kidney of angiotensin II-infused rat. *Lab. Invest. 86*, 1285–1292.

(24) Leveen, P., Pekny, M., Gebre-Medhin, S., Swolin, B., Larsson, E., and Betsholtz, C. (1994) Mice deficient for PDGF B show renal, cardiovascular, and hematological abnormalities. *Genes & development 8*, 1875–1887.

(25) Lindahl, P., Johansson, B. R., Leveen, P., and Betsholtz, C. (1997) Pericyte loss and microaneurysm formation in PDGF-B-deficient mice. *Science (New York, N.Y.) 277*, 242–245.

(26) Soriano, P. (1994) Abnormal kidney development and hematological disorders in PDGF beta-receptor mutant mice. *Genes Dev. 8*, 1888–1896.

(27) Floege, J., Ostendorf, T., Janssen, U., Burg, M., Radeke, H. H., Vargeese, C., Gill, S. C., Green, L. S., and Janjic, N. (1999) Novel approach to specific growth factor inhibition in vivo: antagonism of platelet-derived growth factor in glomerulonephritis by aptamers. *Am. J. Pathol. 154*, 169–179.

(28) Ostendorf, T., Kunter, U., Grone, H. J., Bahlmann, F., Kawachi, H., Shimizu, F., Koch, K. M., Janjic, N., and Floege, J. (2001) Specific antagonism of PDGF prevents renal scarring in experimental glomerulonephritis. *J. Am. Soc. Nephrol. 12*, 909–918.

(29) Gilbert, R. E., Kelly, D. J., McKay, T., Chadban, S., Hill, P. A., Cooper, M. E., Atkins, R. C., and Nikolic-Paterson, D. J. (2001) PDGF signal transduction inhibition ameliorates experimental mesangial proliferative glomerulonephritis. *Kidney Int. 59*, 1324–1332.

(30) Nakamura, H., Isaka, Y., Tsujie, M., Akagi, Y., Sudo, T., Ohno, N., Imai, E., and Hori, M. (2001) Electroporation-mediated PDGF

DOI: 10.1021/bi5015425
Biochemistry 2015, 54, 1918–1929

receptor-IgG chimera gene transfer ameliorates experimental glomerulonephritis. *Kidney Int. 59*, 2134−2145.
(31) Iyoda, M., Shibata, T., Hirai, Y., Kuno, Y., and Akizawa, T. (2011) Nilotinib attenuates renal injury and prolongs survival in chronic kidney disease. *J. Am. Soc. Nephrol. 22*, 1486−1496.
(32) Johnson, R. J., Raines, E. W., Floege, J., Yoshimura, A., Pritzl, P., Alpers, C., and Ross, R. (1992) Inhibition of mesangial cell proliferation and matrix expansion in glomerulonephritis in the rat by antibody to platelet-derived growth factor. *J. Exp. Med. 175*, 1413−1416.
(33) Kinnman, N., Hultcrantz, R., Barbu, V., Rey, C., Wendum, D., Poupon, R., and Housset, C. (2000) PDGF-mediated chemoattraction of hepatic stellate cells by bile duct segments in cholestatic liver injury. *Lab. Invest. 80*, 697−707.
(34) Ogawa, S., Ochi, T., Shimada, H., Inagaki, K., Fujita, I., Nii, A., Moffat, M. A., Katragadda, M., Violand, B. N., Arch, R. H., and Masferrer, J. L. (2010) Anti-PDGF-B monoclonal antibody reduces liver fibrosis development. *Hepatology Res. 40*, 1128−1141.
(35) Borkham-Kamphorst, E., Kovalenko, E., van Roeyen, C. R., Gassler, N., Bomble, M., Ostendorf, T., Floege, J., Gressner, A. M., and Weiskirchen, R. (2008) Platelet-derived growth factor isoform expression in carbon tetrachloride-induced chronic liver injury. *Lab. Invest. 88*, 1090−1100.
(36) Borkham-Kamphorst, E., Stoll, D., Gressner, A. M., and Weiskirchen, R. (2004) Antisense strategy against PDGF B-chain proves effective in preventing experimental liver fibrogenesis. *Biochem. Biophys. Res. Commun. 321*, 413−423.
(37) Czochra, P., Klopcic, B., Meyer, E., Herkel, J., Garcia-Lazaro, J. F., Thieringer, F., Schirmacher, P., Biesterfeld, S., Galle, P. R., Lohse, A. W., and Kanzler, S. (2006) Liver fibrosis induced by hepatic overexpression of PDGF-B in transgenic mice. *J. Hepatol. 45*, 419−428.
(38) Rothe, C., Urlinger, S., Lohning, C., Prassler, J., Stark, Y., Jager, U., Hubner, B., Bardroff, M., Pradel, I., Boss, M., Bittlingmaier, R., Bataa, T., Frisch, C., Brocks, B., Honegger, A., and Urban, M. (2008) The human combinatorial antibody library HuCAL GOLD combines diversification of all six CDRs according to the natural immune system with a novel display method for efficient selection of high-affinity antibodies. *J. Mol. Biol. 376*, 1182−1200.
(39) Prassler, J., Steidl, S., and Urlinger, S. (2009) In vitro affinity maturation of HuCAL antibodies: complementarity determining region exchange and RapMAT technology. *Immunotherapy 1*, 571−583.
(40) Steidl, S., Ratsch, O., Brocks, B., Durr, M., and Thomassen-Wolf, E. (2008) In vitro affinity maturation of human GM-CSF antibodies by targeted CDR-diversification. *Mol. Immunol. 46*, 135−144.
(41) Rauchenberger, R., Borges, E., Thomassen-Wolf, E., Rom, E., Adar, R., Yaniv, Y., Malka, M., Chumakov, I., Kotzer, S., Resnitzky, D., Knappik, A., Reiffert, S., Prassler, J., Jury, K., Waldherr, D., Bauer, S., Kretzschmar, T., Yayon, A., and Rothe, C. (2003) Human combinatorial Fab library yielding specific and functional antibodies against the human fibroblast growth factor receptor 3. *J. Biol. Chem. 278*, 38194−38205.
(42) Tiller, T., Schuster, I., Deppe, D., Siegers, K., Strohner, R., Herrmann, T., Berenguer, M., Poujol, D., Stehle, J., Stark, Y., Hessling, M., Daubert, D., Felderer, K., Kaden, S., Kolln, J., Enzelberger, M., and Urlinger, S. (2013) A fully synthetic human Fab antibody library based on fixed VH/VL framework pairings with favorable biophysical properties. *mAbs 5*, 445−470.
(43) Duncan, A. R., and Winter, G. (1988) The binding site for C1q on IgG. *Nature 332*, 738−740.
(44) Ishino, T., Wang, M., Mosyak, L., Tam, A., Duan, W., Svenson, K., Joyce, A., O'Hara, D. M., Lin, L., Somers, W. S., and Kriz, R. (2013) Engineering a Monomeric Fc Modality by N-Glycosylation for the Half-Life Extension of Biotherapeutics. *J. Biol. Chem. 288*, 16529−16537.
(45) Vonrhein, C., Flensburg, C., Keller, P., Sharff, A., Smart, O., Paciorek, W., Womack, T., and Bricogne, G. (2011) Data processing and analysis with the autoPROC toolbox. *Acta Crystallogr., Sect. D, Biol. Crystallogr. 67*, 293−302.
(46) Evans, P. (2006) Scaling and assessment of data quality. *Acta Crystallogr., Section D, Biol. Crystallogr. 62*, 72−82.
(47) McCoy, A. J., Grosse-Kunstleve, R. W., Adams, P. D., Winn, M. D., Storoni, L. C., and Read, R. J. (2007) Phaser crystallographic software. *J. Appl. Crystallogr. 40*, 658−674.
(48) Blanc, E., Roversi, P., Vonrhein, C., Flensburg, C., Lea, S. M., and Bricogne, G. (2004) Refinement of severely incomplete structures with maximum likelihood in BUSTER-TNT. *Acta Crystallogr., Section D, Biol. Crystallogr. 60*, 2210−2221.
(49) Thompson, J. D., Higgins, D. G., and Gibson, T. J. (1994) CLUSTAL W: improving the sensitivity of progressive multiple sequence alignment through sequence weighting, position-specific gap penalties and weight matrix choice. *Nucleic Acids Res. 22*, 4673−4680.
(50) Sanchez, R., and Sali, A. (1997) Evaluation of comparative protein structure modeling by MODELLER-3. *Proteins Suppl. 1*, 50−58.
(51) Myszka, D. G. (1999) Improving biosensor analysis. *J. Mol. Recognit. 12*, 279−284.
(52) Arunlakshana, O., and Schild, H. O. (1959) Some quantitative uses of drug antagonists. *Br. J. Pharmacol. Chemother. 14*, 48−58.
(53) Knappik, A., Ge, L., Honegger, A., Pack, P., Fischer, M., Wellnhofer, G., Hoess, A., Wolle, J., Pluckthun, A., and Virnekas, B. (2000) Fully synthetic human combinatorial antibody libraries (HuCAL) based on modular consensus frameworks and CDRs randomized with trinucleotides. *J. Mol. Biol. 296*, 57−86.
(54) Shim, A. H., Liu, H., Focia, P. J., Chen, X., Lin, P. C., and He, X. (2010) Structures of a platelet-derived growth factor/propeptide complex and a platelet-derived growth factor/receptor complex. *Proc. Natl. Acad. Sci. U.S.A. 107*, 11307−11312.
(55) Oefner, C., D'Arcy, A., Winkler, F. K., Eggimann, B., and Hosang, M. (1992) Crystal structure of human platelet-derived growth factor BB. *EMBO J. 11*, 3921−3926.
(56) Davies, D. R., Gelinas, A. D., Zhang, C., Rohloff, J. C., Carter, J. D., O'Connell, D., Waugh, S. M., Wolk, S. K., Mayfield, W. S., Burgin, A. B., Edwards, T. E., Stewart, L. J., Gold, L., Janjic, N., and Jarvis, T. C. (2012) Unique motifs and hydrophobic interactions shape the binding of modified DNA ligands to protein targets. *Proc. Natl. Acad. Sci. U. S. A. 109*, 19971−19976.
(57) Ebert, M., Kasper, H. U., Hernberg, S., Friess, H., Buchler, M. W., Roessner, A., Korc, M., and Malfertheiner, P. (1998) Overexpression of platelet-derived growth factor (PDGF) B chain and type beta PDGF receptor in human chronic pancreatitis. *Digest. Dis. Sci. 43*, 567−574.
(58) Pinzani, M., Milani, S., Herbst, H., DeFranco, R., Grappone, C., Gentilini, A., Caligiuri, A., Pellegrini, G., Ngo, D. V., Romanelli, R. G., and Gentilini, P. (1996) Expression of platelet-derived growth factor and its receptors in normal human liver and during active hepatic fibrogenesis. *Am. J. Pathol. 148*, 785−800.
(59) Zheng, X. Y., Zhang, J. Z., Tu, P., and Ma, S. Q. (1998) Expression of platelet-derived growth factor B-chain and platelet-derived growth factor beta-receptor in fibroblasts of scleroderma. *J. Dermatol. Sci. 18*, 90−97.
(60) Yoshida, S., Liu, S., Chung, J., Sverdlov, D. Y., Miyamoto, M., Kim, Y. O., Ogawa, S., Arch, R. H., Schuppan, D., Popov, Y. Extrahepatic supply of PDGF-BB by platelets drives hepatic stellate cell activation and biliary liver fibrosis progression, submitted.
(61) Selzer, T., and Schreiber, G. (2001) New insights into the mechanism of protein-protein association. *Proteins 45*, 190−198.
(62) Cho, H. S., Mason, K., Ramyar, K. X., Stanley, A. M., Gabelli, S. B., Denney, D. W., Jr., and Leahy, D. J. (2003) Structure of the extracellular region of HER2 alone and in complex with the Herceptin Fab. *Nature 421*, 756−760.
(63) Shaw, S., Bourne, T., Meier, C., Carrington, B., Gelinas, R., Henry, A., Popplewell, A., Adams, R., Baker, T., Rapecki, S., Marshall, D., Moore, A., Neale, H., and Lawson, A. (2014) Discovery and characterization of olokizumab: A humanized antibody targeting interleukin-6 and neutralizing gp130-signaling. *mAbs 6*, 774−782.

DOI: 10.1021/bi5015425
Biochemistry 2015, 54, 1918−1929